

Alteration of brain viscoelasticity after shunt treatment in normal pressure hydrocephalus

Florian Baptist Freimann · Kaspar-Josche Streitberger · Dieter Klatt · Kui Lin · Joyce McLaughlin · Jürgen Braun · Christian Sprung · Ingolf Sack

Received: 7 March 2011 / Accepted: 5 April 2011
© Springer-Verlag 2011

Abstract

Introduction Normal pressure hydrocephalus (NPH) represents a chronic neurological disorder with increasing incidence. The symptoms of NPH may be relieved by surgically implanting a ventriculoperitoneal shunt to drain excess cerebrospinal fluid. However, the pathogenesis of NPH is not yet fully elucidated, and the clinical response of shunt treatment is hard to predict. According to current theories of NPH, altered mechanical properties of brain tissue seem to play an important role. Magnetic resonance elastography (MRE) is a unique method for measuring in vivo brain mechanics.

Methods In this study cerebral MRE was applied to test the viscoelastic properties of the brain in 20 patients with

primary ($N=14$) and secondary ($N=6$) NPH prior and after (91 ± 16 days) shunt placement. Viscoelastic parameters were derived from the complex modulus according to the rheological springpot model. This model provided two independent parameters μ and α , related to the inherent rigidity and topology of the mechanical network of brain tissue.

Results The viscoelastic parameters μ and α were found to be decreased with -25% and -10% , respectively, compared to age-matched controls ($P<0.001$). Interestingly, α increased after shunt placement ($P<0.001$) to almost normal values whereas μ remained symptomatically low.

Conclusion The results indicate the fundamental role of altered viscoelastic properties of brain tissue during disease progression and tissue repair in NPH. Clinical improvement in NPH is associated with an increasing complexity of the mechanical network whose inherent strength, however, remains degraded.

Florian Baptist Freimann and Kaspar-Josche Streitberger have contributed equally to this work.

F. B. Freimann · C. Sprung (✉)
Neurosurgical Department, Charité—University Medicine Berlin,
Campus Virchow-Klinikum,
13353 Berlin, Germany
e-mail: christian.sprung@charite.de

K.-J. Streitberger · D. Klatt · I. Sack (✉)
Department of Radiology, Charité—University Medicine Berlin,
Campus Charité Mitte,
Charitéplatz 1,
10117 Berlin, Germany
e-mail: ingolf.sack@charite.de

K. Lin · J. McLaughlin
Mathematics Department, Rensselaer Polytechnic Institute,
Troy, NY, USA

J. Braun
Institute of Medical Informatics, Charité—University Medicine
Campus Benjamin Franklin,
12200 Berlin, Germany

Keywords Normal pressure hydrocephalus · Shunt · Magnetic resonance elastography (MRE) · Viscoelasticity · Springpot

Introduction

The pathophysiology of normal pressure hydrocephalus (NPH) is still a matter of controversy and intensive research. It is accepted that cerebrospinal fluid (CSF) flow, CSF resorption, and intracranial cavity pressure are altered in NPH [1–4]. However, the role of parenchymal changes to pathogenesis and symptoms in NPH remains unclear. The complexity of the pathophysiology underlying NPH arises from a cascade of events including metabolic changes, altered blood flow, impaired CSF exchange, and

intracranial pressure peaks which expedite parenchymal degradation and functional disorder [5–7]. NPH represents one of the rare chronic neurological disorders whose symptoms may be relieved by surgical intervention. In many cases, implantation of a shunt that drains CSF excess improves typical NPH-symptoms given by Hakim's Triad (gait disturbance, dementia, and urinary incontinence) [8]. However, the prognosis of the interventional NPH treatment is still difficult due to unknown inciting etiology and unclear pathogenesis. Neuroradiological markers like Evan's index (the maximal frontal horn ventricular width divided by the transverse inner diameter of the skull) may support the diagnosis of NPH by providing morphology-based thresholds but are of limited sensitivity to the inherent structure of brain parenchyma at multiple scales [9]. Recently, magnetic resonance elastography (MRE) [10] has been proven to be particularly useful for translating microstructural changes inside the mechanical network of the brain into a global imaging contrast [11–14]. Since mechanical parameters such as tissue compression and CSF dynamics seem to play an important role in NPH, in vivo viscoelastic constants of the brain may reveal pathophysiological details not accessible by conventional imaging methods.

In this study, recently introduced multifrequency MRE [15–17] is used to investigate the alteration of the viscoelasticity of brain tissue in NPH associated with the rehabilitation of clinical symptoms after shunt placement. The hypothesis is that throughout the pathological cascade in NPH, several processes impact the viscoelastic properties of brain which might be reversed by tissue repair after shunt implantation. In a previous study, a group of 20 patients suffering from NPH was investigated by MRE combined with rheological parameter fitting of the measured complex modulus dispersion function [17]. Using the two-parameter springpot model, it was demonstrated that both the shear modulus μ (with the dimension of kilopascal) and α (the dimensionless power of the springpot-inherent powerlaw) decrease due to NPH. The springpot is an interpolation between pure elastic material behavior modeled by a spring and a viscose fluid modeled by a dashpot element. μ can be interpreted as a measure of elastic stiffness with comparison with “stiff” (high μ values) and “soft” (low μ values) materials. α is related to the slope of the complex shear modulus (in the following called G^* -dispersion) and is thus influenced by the inherent network structure. To further illustrate this, α is low in a pudding-like material such as a gel. There the material consists of few but long (almost one dimensional, i.e., weakly linked) fibers within the percolation limit. In contrast, biological tissue has a highly linked three-dimensional (3D) network structure determined, e.g., by vascular trees or collagen or neuronal networks. The

dimensionality (or more generally the fractal dimension) of the mechanical network is higher in biological materials than in weakly linked gels [18], causing higher values for the α parameter in tissue [19]. This higher value corresponds to a larger imaginary part of the complex modulus and is consistent with the absorption of mechanical energy.

The current study analyzes the mechanical network structure of the brain by means of μ and α . Therefore, 20 patients have been investigated using a similar multifrequency MRE protocol as has been used in a previous study of MRE in NPH [17]. In our current protocol, no healthy controls were included. However, for the purpose of comparison, data of [17] are taken and plotted against current findings. Our study aims to shed light into the complex interaction between brain mechanics, NPH symptoms, and rehabilitation after shunting. Moreover, we will report modulus data at four mechanical drive frequencies intended as a database for mechanical modeling in hydrocephalus.

Materials and methods

Patients

The study was approved by the local ethics committee (protocol No EA1/246/09). Written informed consent was obtained from all patients prior to the investigation. Twenty patients with primary ($N=14$) and secondary ($N=6$) NPH were selected in the study (mean age 71 years, standard deviation [SD] 9 years; age range 51–85 years; 8 males, 12 females) based on the following criteria: incidence of at least two clinical symptoms of Hakim's Triad, associated with typical radiological findings of NPH (hydrocephalic ventricles with an Evan's index greater or equal than 0.3, effaced cortical sulci and missing signs of severe atrophy or leukoencephalopathy). Patients with any psychiatric disease, cerebral infarction, brain tumor, and those with hydrocephalus following severe cerebral hemorrhage or infections within the last 6 months were excluded. Gait disturbance, bladder incontinence, and dementia were evaluated using the grading system established by Mori [20]. Preoperative MRE was followed by a continuous external CSF drainage (10 ml/h) using a lumbar catheter for 48 h. In case of unequivocal clinical improvement following lumbar CSF drainage, a ventriculoperitoneal shunt including programmable valves (Fa. Miethke; Potsdam, Germany) with initial opening pressure of 5 cmH₂O inside the adjustment unit and 20 cmH₂O shunt assistant was implanted. In case of a suspected functional underdrainage, the opening pressure was readjusted to enhance the clinical improvement [21]. In none of the 20 patients included in this study, a revision of the shunt or an increase of the pressure

setting due to overdrainage was necessary. Clinical evaluation and MRE were repeated 92 ± 17 days after shunt surgery.

Cerebral MRE

The major steps of an MRE experiment are displayed in Fig. 1. Measurements were performed on a standard 1.5-T clinical MRI scanner (Sonata; Siemens, Erlangen, Germany). Mechanical vibrations were induced into the head by a custom-made head cradle connected via carbon-fiber piston to a remote vibration generator as described in [12]. The vibration waveform was synthesized by a superposition of

four harmonic oscillations of 25, 37.5, 50, and 62.5 Hz frequency with equal phases and a total duration of 400 ms [11]. A single burst of this signal was fed into the wave generator prior to the start of each image acquisition. Wave images were acquired using a spin echo echo-planar imaging sequence which was sensitized to motion by a sinusoidal motion-encoding gradient (MEG) during the first half of the echo period. The center frequency of the MEG was 60 Hz by a length of the MEG of four periods equal to 66.67 ms and an amplitude of 35 mT/m in through-plane direction. The polarity of the MEG was toggled in each second experiment for subtracting the inverse phase contrast and leaving the

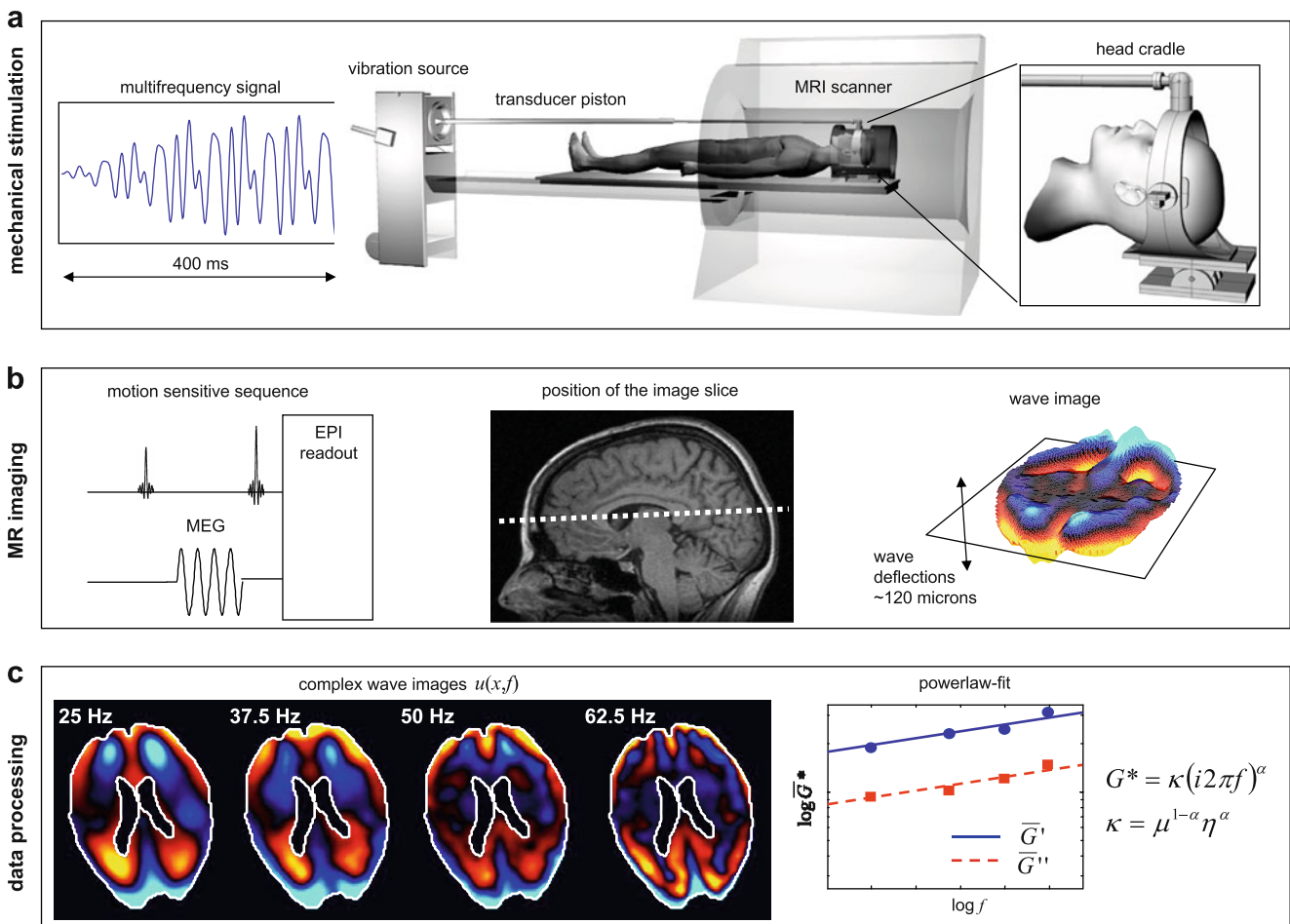


Fig. 1 Scheme of a typical multifrequency MRE experiment of human brain. **a** The MRI scanner is combined with a device for acoustical head stimulations comprising: (1) a signal generator that produces a multifrequency waveform composed from four harmonic vibrations of 25, 37.5, 50, and 62.5 Hz frequency; (2) a loudspeaker for generating the acoustic vibrations; (3) an extended piston that transfers the vibrations into the scanner; and (4) a head cradle for stimulating head vibrations mainly along the head–feet direction. **b** A single-shot EPI sequence is sensitized to harmonic motions by a 60-Hz sinusoidal MEG of 4 cycles with a direction through the image plane. The image plane is positioned in transverse orientation through the brain, parallel to the genu and splenium of the corpus callosum. The resulting wave images display the motion component along the

head–feet direction corresponding to the major vibration direction of the actuator. **c** Image processing comprises Fourier decomposition of the superposed oscillations yielding four complex single-frequency wave images $u(x, f)$ corresponding to the experimentally applied vibration frequencies. Each of the wave images is separately inverted resulting in four complex-valued shear modulus images $G^*(x, f)$ whose values are averaged within a region of interest comprising the parenchyma within the image slice (demarcated in the wave images by white lines). A combined fit of both real part and imaginary part of $G^*(f)$ according to the springpot model yields two viscoelastic parameters: The shear modulus $\bar{\mu}$ and the powerlaw exponent $\bar{\alpha}$ associated to the topology of the underlying micromechanical network (henceforth called connectivity parameter)

difference wave phase in the image. The experiment was repeated in order to capture the dynamics of wave propagation. Therefore, the delay between the onset of vibration and the start of motion encoding was varied 32 times from 320.0 to 397.5 ms by an increment of 2.5 ms. The resulting phase shift corresponds to a first harmonic frequency of 12.5 Hz which determines the resolution in our vibration spectrum. One transverse image slice of 6 mm thickness was selected through the central part through the ventricles parallel to the internal base of the skull. Further image acquisition parameters were: repetition time TR, 3 s; echo time TE, 149 ms; field of view (FoV), 192×192 mm²; and matrix size 128×128.

Data evaluation

For data analysis, the time traces of the waves at each planar spatial point \mathbf{x} were Fourier transformed to create the time-harmonic, complex out-of-image plane displacement $u(\mathbf{x}, f)$ at each of the mechanical driving frequencies, $f=25, 37.5, 50, \text{ and } 62.5 \text{ Hz}$.

Brain biomechanics comparisons are reported based on the complex shear modulus, $G^*(\mathbf{x}, f)$, in the parenchyma excluding the ventricles. Using a locally constant assumption for the complex modulus, $G^*(\mathbf{x}, f)$, the relationship,

$$G^*(\mathbf{x}, f) = -(2\pi f)^2 \rho u(\mathbf{x}, f) / \Delta u(\mathbf{x}, f), \tag{1}$$

where $\rho=1,000 \text{ kg/m}^3$ is the tissue density within the brain parenchyma, was used to calculate $G^*(\mathbf{x}, f)$ at each frequency. The global $\overline{G}^*(f)$ was calculated by averaging $G^*(\mathbf{x}, f)$ over all parenchyma spatial points. The complex-modulus according to the springpot model is given by

$$\overline{G}^*(f) = \overline{\kappa}(2\pi f i)^{\overline{\alpha}} \tag{2}$$

where $\overline{\kappa} = \overline{\mu}^{1-\overline{\alpha}} \overline{\eta}^{\overline{\alpha}}$, and $\overline{\kappa}$ and $\overline{\alpha}$ are frequency independent. The parameter $\overline{\mu}$ is the global shear elasticity, $\overline{\eta}$ is the viscous damping, and $\overline{\alpha}$ is a measure of the elastic lossy relation. For example, $\overline{\alpha} = 0$ corresponds to lossless elastic behavior with shear elasticity, $\overline{\mu}$ and $\overline{\alpha} = 1$ to lossy viscous damping with viscosity, $\overline{\eta}$. The global storage modulus $\overline{G}'(f) = \text{Re}\overline{G}^*(f)$ and the global loss modulus $\overline{G}''(f) = \text{Im}\overline{G}^*(f)$ are tabulated. The parameters $\overline{\kappa}$ and $\overline{\alpha}$ were determined by a least square fit over frequency of the tabulated global $\overline{G}^*(f)$ using the springpot model. We present tables of $\overline{G}'(f)$, $\overline{G}''(f)$, the ratio $\overline{G}''(f)/\overline{G}'(f)$, $\overline{\alpha}$ and $\overline{\mu}$ where for the latter tabulation we assume $\overline{\eta} = 3.7 \text{ Pa}$. This value of $\overline{\eta}$ was previously determined as an approximated value of viscosity in human brain tissue [15]. Statistical hypotheses were tested by a two-sided Student's t test. The level of significance was 0.05. For statistical analysis the Matlab R2007b statistics toolbox was used.

Results

Shunt surgery yielded a significant improvement of the clinical score according to [20] from 6 ± 3 to 3 ± 2 ($P=0.001$). In contrast, the change in Evan's indices was statistically not significant as represented by mean values for the pre- and postoperation indices of 0.37 ± 0.05 and 0.35 ± 0.05 ($P=0.23$). Individual clinical and neuroradiological scores are given in Table 1.

MRE was successfully performed in all patients without any complication and discomfort. The mean elasticity $\overline{\mu}$ of all patients prior to shunt treatment was $2.24\pm 0.38 \text{ kPa}$. Ninety days after shunt implantation, $\overline{\mu} = 2.26 \pm 0.41 \text{ kPa}$ and so $\overline{\mu}$ remained unchanged after shunt treatment (Fig. 2). This insensitivity of $\overline{\mu}$ is corroborated by \overline{G}' given in Table 2 which does not significantly change with shunt implantation ($P>0.05$). The situation changes when the mechanical energy loss in \overline{G}'' is taken into account. \overline{G}'' at

Table 1 Clinical data of each patient included in this study

No.	NPH	Sex	Age (years)	Δt (days)	Clinical score pre-shunt	Clinical score post-shunt	Evan's index pre-shunt	Evan's index post-shunt
1	p	f	71	90	6	1	0.36	0.34
2	s	f	76	91	3	1	0.34	0.33
3	s	m	51	92	12	1	0.42	0.40
4	p	m	66	91	4	4	0.48	0.47
5	p	f	66	84	9	7	0.35	0.32
6	p	f	70	89	1	0	0.46	0.44
7	s	f	69	105	4	0	0.4	0.25
8	p	m	72	99	5	1	0.39	0.38
9	p	f	77	71	6	4	0.32	0.32
10	s	m	85	60	6	5	0.36	0.34
11	p	m	83	91	6	4	0.36	0.32
12	p	f	79	91	5	3	0.36	0.36
13	p	f	80	85	8	8	0.38	0.38
14	s	f	60	78	1	0	0.37	0.34
15	p	m	76	147	5	3	0.37	0.37
16	p	m	66	92	5	3	0.29	0.29
17	s	m	79	98	11	5	0.34	0.34
18	p	f	53	92	7	2	0.35	0.34
19	p	f	65	91	5	4	0.29	0.29
20	p	f	71	104	5	1	0.33	0.32
mean			71	92	6	3	0.37	0.35
SD			9	17	3	2	0.05	0.05
					$P=0.0010857$		$P=0.23081$	
					$R=0.49765$		$R=0.19381$	

Types of NPH are either primary (p) or secondary (s)
 Δt delay between both MRE examinations, R Pearson's correlation coefficient

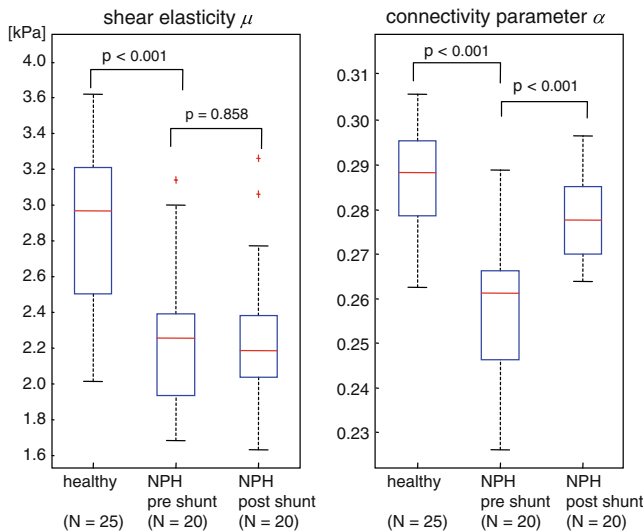


Fig. 2 Brain viscoelastic parameters $\bar{\mu}$ and $\bar{\alpha}$ according to the springpot model in healthy volunteers (data taken from [17]) and in NPH prior and after shunting. The *boxplot* depicts the lower and upper quartiles as well as the 50th percentile (median). Full data range is presented by the *whiskers*

25 Hz displays a significant increase with shunt treatment. The change in the loss properties of tissue is directly represented by the ratio \bar{G}''/\bar{G}' which is also called the loss tangent. The loss tangent is related to the springpot model by $\bar{\alpha} = 2/\pi \arctan(\bar{G}''/\bar{G}')$ provided that the ratio \bar{G}''/\bar{G}' is constant over frequency. A highly significant shunt-related increase of the loss tangent, as calculated by the above formula, was observed at low drive frequencies (25 and 37.5 Hz). However, for our rheology model, $\bar{\alpha}$ is frequency independent; hence, we found $\bar{\alpha}$ by fitting all the

data using the relation $\bar{G}^*(f) = \bar{\kappa}(2\pi fi)^{\bar{\alpha}}$. This method has the added positive feature that it better compensates for experimental variability of \bar{G}' and \bar{G}'' as well as producing a frequency-independent $\bar{\alpha}$. This fit-based evaluation yielded $\bar{\alpha} = 0.258 \pm 0.014$ and $\bar{\alpha} = 0.279 \pm 0.009$ for pre- and posttreatment, respectively ($P < 0.00001$, Fig. 2). The correlation of $\bar{\alpha}$ with patient treatment might even be increased by limiting the data of the springpot fit to 25 and 37.5-Hz moduli yielding an increase in Pearson's correlation coefficient from 0.65 (full frequency range) to 0.73. In this low-frequency range the evaluation yielded $\bar{\alpha} = 0.238 \pm 0.013$ prior treatment and $\bar{\alpha} = 0.271 \pm 0.018$ with shunt ($P < 0.00001$).

Discussion

Since Hakim's first report of NPH symptoms in 1965 [22], many theories on the underlying pathophysiology of NPH were discussed. Animal experiments have been performed where functional stenosis of the aqueduct is produced following abnormal ventricular systole. This was accomplished by inducing an elevated aqueductal CSF flow and intracranial pressure peaks [23]. Hydrodynamic events are accompanied by metabolic malfunction including decreased blood flow in periventricular regions [5, 24, 25] and reduced drainage of toxic metabolites [6, 7]. Until now the inciting event of the pathological cascade of NPH is unclear and the mechanisms of rehabilitation after shunt treatment remain speculative.

Our study adds novel information to this puzzle by providing data of brain mechanical properties in NPH at disease state and during recovery. Recently, a decrease in $\bar{\mu}$

Table 2 Storage moduli G' , loss moduli G'' , and springpot model parameters μ and α (the standard deviation is given in brackets)

	NPH pretreatment	NPH posttreatment	P value	R
Complex moduli				
G' (25.0 Hz) ^a	1.29 (0.20)	1.36 (0.20)	0.29402	0.175
G' (37.5 Hz) ^a	1.64 (0.21)	1.55 (0.22)	0.20594	-0.210
G' (50.0 Hz) ^a	1.72 (0.22)	1.64 (0.22)	0.26732	-0.185
G' (62.5 Hz) ^a	2.18 (0.31)	2.01 (0.25)	0.06618	-0.301
G'' (25.0 Hz) ^a	0.51 (0.09)	0.63 (0.12)	0.00155	0.496
G'' (37.5 Hz) ^a	0.63 (0.09)	0.68 (0.11)	0.10875	0.264
G'' (50.0 Hz) ^a	0.80 (0.13)	0.80 (0.13)	0.96918	-0.006
G'' (62.5 Hz) ^a	1.02 (0.19)	0.96 (0.15)	0.27634	-0.181
Modulus ratios				
G''/G' (25 Hz)	0.40 (0.03)	0.46 (0.06)	0.00012	0.585
G''/G' (37.5 Hz)	0.38 (0.03)	0.44 (0.04)	0.00002	0.636
G''/G' (50 Hz)	0.47 (0.05)	0.49 (0.03)	0.12571	0.253
G''/G' (62.5 Hz)	0.47 (0.04)	0.48 (0.03)	0.42685	0.133
Springpot model parameters				
μ^a	2.24 (0.38)	2.26 (0.41)	0.85811	0.03
α	0.258 (0.014)	0.279 (0.009)	<0.00001	0.65

P values refer to differences between both groups of patients pre- and post-shunt implantation

R Pearson's correlation coefficient

^a In kilopascal

and $\bar{\alpha}$ due to NPH was reported [17] with $\bar{\mu}$ changing from 2.84 ± 0.44 kPa (healthy controls) to 2.27 ± 0.24 kPa (Patients), which represents a loss in brain stiffness about 25.1%. Data of 12 patients of this prior study [17] were included in the pre-shunt group of the present study. In this prior study, the same mathematical model, Eqs. 1 and 2, that relates the out-of-image plane displacement with the complex shear modulus and the biomechanical parameters $\bar{\mu}$ and $\bar{\alpha}$, is used.

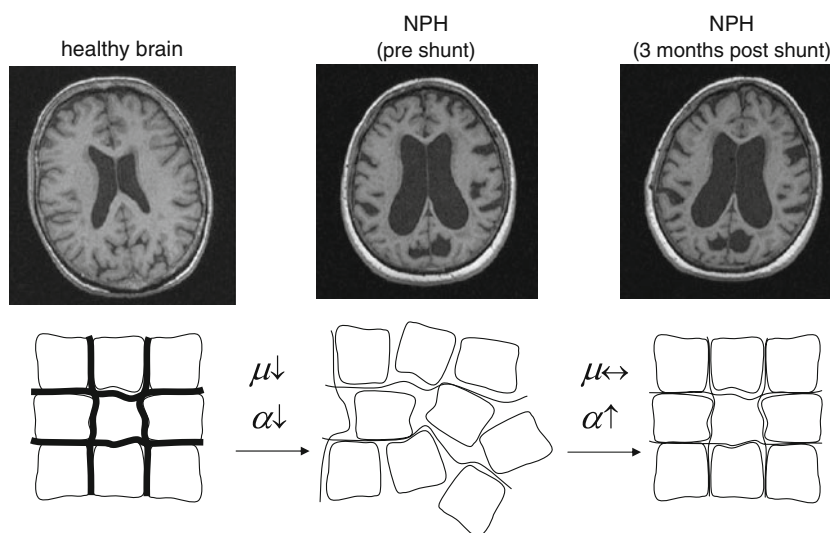
Before continuing with our comparison of results, we comment on our mathematical model. In this model we start with a linear viscoelastic model and then we have made several simplifications: (1) the first is that we assume that the biomechanical parameters vary in only the directions tangent to the image plane; (2) then, we eliminate the term in the elastic system that corresponds to the dilatational (or volumetric) changes; one argument for this is that shear deformation is volume conservative; even so, there is interplay between compression and shear deformation, so this simplification may have some effect on our average properties; (3) we assume that the fluid and solid matrix move together, that is, there is no relative motion; and finally, (4) we make a locally constant assumption. All of our assumptions result in the decoupling of the equations that govern the three displacement components and reduce our mathematical model for the out-of-plane displacement to the form Eq. 1.

Returning to our comparison, we note that in the present study only a single image slice was used for spatially averaging the tabulated viscoelastic parameters. In [17] the model Eqs. 1 and 2 was also used as the governing equation for the out-of-plane component; there, we utilized data for three slices in planar multifrequency MRE and averaged the biomechanical parameters over all three slices. It is remarkable that when the target is average biomechanical

parameters and we make the assumptions given above, the average biomechanical parameters determined by averaging over a single slice, which we do here, are so similar to the average biomechanical parameters found by averaging over three parallel slices [17].

Compared to the control data of [17], we now observed a loss in $\bar{\mu}$ by 26.8% ($P=0.00001$, $R=-0.61$) pre-shunt and by 25.7% ($P=0.00003$, $R=-0.58$) post-shunt. By $\bar{\alpha}$ we measured 0.279 ± 0.009 for recovered brain which is slightly lower (-3% , $P=0.0139$) than what was found in [17] for healthy controls ($\bar{\alpha} = 0.287 \pm 0.011$). In contrast, $\bar{\alpha}$ in our present pre-shunting group was 0.258 ± 0.014 which is not different ($P=0.3017$) from what has been reported in [17] ($\bar{\alpha} = 0.262 \pm 0.011$, $\Delta\bar{\alpha} \approx -10\%$). The significantly lower $\bar{\alpha}$ in patients who underwent shunting compared to healthy volunteers is remarkable as it might indicate that tissue repair is not fully accomplished 3 months after shunt placement. According to the theory of generalized Gaussian structures, the α parameter is sensitive to the geometry of the mechanical network [26]. Within the intermediate frequency range of the complex modulus (the so-called scaling range), α is directly related to the spectral dimension, i.e., the generalization of the integer-valued Euclidian dimension of fractal structures. As has been illustrated in [27], α increases with an increasing number of vibration freedoms in the network, which is, e.g., the case when myosin bridges are established in skeletal muscle upon contraction. Then, however, also μ increases as the muscle hardens [27]. It is most intriguing that tissue repair in NPH is not associated with an increase in μ . We interpret the symptomatically low μ in untreated NPH as a signature of tissue degeneration following multiple chronic stresses to the mechanical matrix of the tissue. It is an interesting result of this study that reduction of chronic stress on the ventricular walls by continuous CSF drainage does not

Fig. 3 NPH is associated with ventriculomegaly which is not necessarily recovered after shunting. Cerebral MRE reveals a disease-related decrease in global brain stiffness indicated by μ , which is not improved by shunt treatment. In contrast α increases 3 months after shunt implantation to almost asymptomatic values which suggests that the topology of the mechanical tissue matrix is reorganized while its inherent strength remains degraded



reverse tissue degeneration in the sense of re-establishing the former mechanical strength in the tissue. However, an increasing α due to CSF drainage indicates mechanical reordering, i.e., the dimensionality of a hierarchic network increases or, in other words, the number of the micro-mechanical connections inside the tissue is restored by shunt treatment. This interpretation of our results is illustrated in Fig. 3. It is seen that morphology as ventricle size (quantified by Evan's index in Table 1) does apparently not alter with shunting. The alteration of α may provide a novel neuroradiological marker for therapy monitoring in NPH. To date there are only few neuroimaging markers which significantly change due to tissue repair in NPH and thus have a potential predictive value for NPH treatment [28]. Most notably, magnetic resonance spectroscopy was reported to correlate with the clinical response of shunting [29], whereas in diffusion tensor imaging, similar to our data, no statistically linear correlation to the degree of symptoms was found [30]. The anisotropy of water diffusivity in NPH increases due to hydrostatic compression especially in white matter tracts located around the lateral ventricles [30].

Alternatively, if in the future we take into account dilatational tissue vibrations using 3D tensor MRE and a poroviscoelastic model, this will allow us to determine any impact the more advanced model has on the computed shear modulus and furthermore enable us to deduce poroelastic constants which reflect how compression properties of a sponge-like tissue model induce motion of the fluid relative to the solid. We anticipate that such pressure-related mechanical parameters are highly correlated to the state of the disease and may thus help identify those patients who would benefit from shunt surgery.

However, to date multifrequency 3D tensor MRE is a time-consuming imaging technique whose clinical applicability remains to be tested in future studies. Another limitation of the present study is the lacking spatial resolution. In general, modulus recovery from wave data requires the solution of inverse problems which is mathematically ill-posed and therefore, the calculated G^* maps are inherently limited in their spatial resolution. For this reason brain MRE has provided most consistent data by averaging $G^*(\mathbf{x}, f)$ over all parenchyma spatial points to global $\bar{G}^*(f)$ measures. In [17] a preliminary conclusion about local variations in $\bar{\mu}$ and $\bar{\alpha}$ was drawn by comparing values averaged within a region of interest related to periventricular spaces with global values. While in [17] a higher correlation of $\bar{\mu}$ and $\bar{\alpha}$ to NPH was observed inside the periventricular ROI, a similar spatial constraint in the present study indicated that there is no enhanced effect of tissue repair inside the periventricular spaces. However, any considerations of effects derived from spatially resolved modulus maps in MRE need further work on the improvement of data recovery from time-harmonic wave images.

Conclusions

Our study has shown that tissue repair in NPH following shunt surgery is associated with mechanical reordering of brain tissue but does not influence cerebral shear elasticity which is about 25% lower in symptomatic brain compared to age-matched controls. This reorganization of tissue is not seen by morphology-based parameters but reflects subtle processes of tissue inherent restructuring which are scaled into the frequency power-law of the global shear modulus. In NPH patients the powerlaw exponent α is about 10% lower than in normal brain and remains slightly decreased (−3%) 3 months after shunting, indicating that reorder processes in the brain have not yet fully accomplished.

Conflict of interest We declare that we have no conflict of interest.

References

- Hakim S, Venegas JG, Burton JD (1976) The physics of the cranial cavity, hydrocephalus and normal pressure hydrocephalus: mechanical interpretation and mathematical model. *Surg Neurol* 5(3):187–210
- Levine DN (2008) Intracranial pressure and ventricular expansion in hydrocephalus: have we been asking the wrong question? *J Neurol Sci* 269(1–2):1–11
- Penn RD, Linninger A (2009) The physics of hydrocephalus. *Pediatr Neurosurg* 45(3):161–174
- Yamashita F, Sasaki M, Takahashi S, Matsuda H, Kudo K, Narumi S, Terayama Y, Asada T (2010) Detection of changes in cerebrospinal fluid space in idiopathic normal pressure hydrocephalus using voxel-based morphometry. *Neuroradiology* 52(5):381–386
- Chang CC, Asada H, Mimura T, Suzuki S (2009) A prospective study of cerebral blood flow and cerebrovascular reactivity to acetazolamide in 162 patients with idiopathic normal-pressure hydrocephalus. *J Neurosurg* 111(3):610–617
- Kondziella D, Sonnewald U, Tullberg M, Wikkelsö C (2008) Brain metabolism in adult chronic hydrocephalus. *J Neurochem* 106(4):1515–1524
- Eide PK, Stanic M (2010) Cerebral microdialysis and intracranial pressure monitoring in patients with idiopathic normal-pressure hydrocephalus: association with clinical response to extended lumbar drainage and shunt surgery. *J Neurosurg* 112(2):414–424
- Hebb AO, Cusimano MD (2001) Idiopathic normal pressure hydrocephalus: a systematic review of diagnosis and outcome. *Neurosurgery* 49(5):1166–1184, discussion 1184–1166
- Graff-Radford NR (2007) Normal pressure hydrocephalus. *Neurol Clin* 25(3):809–832, vii–viii
- Muthupillai R, Lomas DJ, Rossman PJ, Greenleaf JF, Manduca A, Ehman RL (1995) Magnetic resonance elastography by direct visualization of propagating acoustic strain waves. *Science* 269(5232):1854–1857
- Klatt D, Hamhaber U, Asbach P, Braun J, Sack I (2007) Noninvasive assessment of the rheological behavior of human internal organs using multifrequency MR elastography: a study of brain and liver viscoelasticity. *Phys Med Biol* 52(24):7281–7294

12. Sack I, Beierbach B, Hamhaber U, Klatt D, Braun J (2008) Non-invasive measurement of brain viscoelasticity using magnetic resonance elastography. *NMR Biomed* 21(3):265–271
13. Green MA, Bilston LE, Sinkus R (2008) In vivo brain viscoelastic properties measured by magnetic resonance elastography. *NMR Biomed* 21:755–764
14. Kruse SA, Rose GH, Glaser KJ, Manduca A, Felmlee JP, Jack CR Jr, Ehman RL (2008) Magnetic resonance elastography of the brain. *Neuroimage* 39(1):231–237
15. Sack I, Beierbach B, Wuerfel J, Klatt D, Hamhaber U, Papazoglou S, Martus P, Braun J (2009) The impact of aging and gender on brain viscoelasticity. *Neuroimage* 46(3):652–657
16. Wuerfel J, Paul F, Beierbach B, Hamhaber U, Klatt D, Papazoglou S, Zipp F, Martus P, Braun J, Sack I (2010) MR-elastography reveals degradation of tissue integrity in multiple sclerosis. *Neuroimage* 49(3):2520–2525
17. Streitberger KJ, Wiener E, Hoffmann J, Freimann FB, Klatt D, Braun J, Lin K, McLaughlin J, Sprung C, Klingebiel R, Sack I (2010) In vivo viscoelastic properties of the brain in normal pressure hydrocephalus. *NMR Biomed*. doi:10.1002/nbm.1602
18. Mandelbrot BB (1983) *The fractal geometry of nature*, 1st edn. W. H. Freeman and company, New York
19. Riek K, Klatt D, Nuzha H, Mueller S, Neumann U, Sack I, Braun J (2011) Wide-range dynamic magnetic resonance elastography. *J Biomech* 44(7):1380–1386
20. Mori K (2001) Management of idiopathic normal-pressure hydrocephalus: a multiinstitutional study conducted in Japan. *J Neurosurg* 95(6):970–973
21. Sprung C, Miethke C, Schlosser HG, Brock M (2005) The enigma of underdrainage in shunting with hydrostatic valves and possible solutions. *Acta Neurochir Suppl* 95:229–235
22. Hakim S, Adams RD (1965) The special clinical problem of symptomatic hydrocephalus with normal cerebrospinal fluid pressure. Observations on cerebrospinal fluid hydrodynamics. *J Neurol Sci* 2(4):307–327
23. Di Rocco C, Di Trapani G, Pettorossi VE, Caldarelli M (1979) On the pathology of experimental hydrocephalus induced by artificial increase in endoventricular CSF pulse pressure. *Childs brain* 5(2):81–95
24. Owler BK, Momjian S, Czosnyka Z, Czosnyka M, Pena A, Harris NG, Smielewski P, Fryer T, Donovan T, Coles J, Carpenter A, Pickard JD (2004) Normal pressure hydrocephalus and cerebral blood flow: a PET study of baseline values. *J Cereb Blood Flow Metab* 24(1):17–23
25. Krauss JK, Regel JP, Vach W, Orszagh M, Jungling FD, Bohus M, Droste DW (1997) White matter lesions in patients with idiopathic normal pressure hydrocephalus and in an age-matched control group: a comparative study. *Neurosurgery* 40(3):491–495, discussion 495–496
26. Gurtovenko AA, Blumen A (2005) Generalized Gaussian structures: models for polymer systems with complex topologies. In: *Polymer analysis, polymer theory. Advances in polymer science*. vol 182. Springer, Berlin, pp 171–282. doi:10.1007/b135561
27. Klatt D, Papazoglou S, Braun J, Sack I (2010) Viscoelasticity-based magnetic resonance elastography of skeletal muscle. *Phys Med Biol* 55:6445–6459
28. Toma AK, Holl E, Kitchen ND, Watkins LD (2011) Evans' index revisited: the need for an alternative in normal pressure hydrocephalus. *Neurosurgery* 68(4):939–944
29. Shiino A, Nishida Y, Yasuda H, Suzuki M, Matsuda M, Inubushi T (2004) Magnetic resonance spectroscopic determination of a neuronal and axonal marker in white matter predicts reversibility of deficits in secondary normal pressure hydrocephalus. *J Neurol Neurosurg Psychiatry* 75(8):1141–1148
30. Osuka S, Matsushita A, Yamamoto T, Saotome K, Isobe T, Nagatomo Y, Masumoto T, Komatsu Y, Ishikawa E, Matsumura A (2010) Evaluation of ventriculomegaly using diffusion tensor imaging: correlations with chronic hydrocephalus and atrophy. *J Neurosurg* 112(4):832–839